ARTICLES

Benign Decay vs. Photolysis in the Photophysics and Photochemistry of 5-Bromouracil. A Computational Study

Monika Kobyłecka,[†] Annapaola Migani,[‡] David Asturiol,[‡] Janusz Rak,[†] and Lluís Blancafort*[,‡]

Institut de Química Computacional, Departament de Química, Universitat de Girona, Campus de Montilivi, 17071 Girona, Spain, and Department of Chemistry, University of Gdańsk, Sobieskiego 18, Gdańsk 80- 952, Poland

Received: December 22, 2008; Revised Manuscript Received: February 27, 2009

The excited state potential energy surface of 5-bromouracil has been studied with ab initio CASPT2//CASSCF calculations to rationalize the competition between the benign decay and the photolysis found experimentally. The surface is characterized by an extended region of degeneracy between S_1 and S_0. The access to this region has been studied with minimum energy path calculations from the FC structure, the seam of intersection has been mapped in detail, and the decay paths from different regions of the seam have been characterized. There are two decay paths with low barriers that are limiting cases for the actual decay dynamics. The first path involves the bromine elimination and leads to a region of near degeneracy between the ground and excited states, and the second one leads back to the reactant through a conical intersection between the two states. The conical intersection for benign decay is part of a seam that lies along the C_5-Br stretching coordinate, and decay at the region of the seam with a stretched C_5-Br bond leads to photolysis. Thus, the reactivity depends on the point of the seam at which decay to the ground state takes place. The low experimental photolysis quantum yield suggests that the energetically favored decay is the one that regenerates the reactant, while the low barriers computed to access the region of decay are in agreement with the measured picosecond excited state lifetime.

Introduction

UV radiation has a limited damaging potential toward natural DNA because the main photochemical damages (e.g., thymine adducts) can be repaired by enzymes.[1] In contrast, UV irradiation of DNA analogues where a thymine base is replaced by isosteric 5-bromouracil (5-BrU, see Scheme 1) leads to direct strand breaks[2−4] and intra-[5,6] and interstrand[7] photo-cross-links, which are one of the most toxic types of DNA lesions. Therefore, incorporation of halogenated uracil derivatives to DNA provides a strategy for the sensitization of DNA to UV radiation. Moreover, since the halogenated base can be incorporated during the natural DNA biosynthesis in the cell,[8] UV sensitization by means of 5-BrU has a therapeutic potential, in a similar spirit to photodynamic therapy. In addition to that, UV-sensitized DNA has been used to study nucleoprotein photo-cross-linking.[9−12]

The mechanism postulated for UV-induced DNA damage[2−4] starts with the photoinduced electron transfer from an adjacent purine base to the 5-bromouracil unit, followed by loss of a bromine anion and formation of a uridin-5-yl radical. This species initiates the strand damage by abstraction of the C2′ hydrogen from the sugar moiety of the adjacent purine base. While the mechanistic aspects of this reaction sequence are largely unclear, the photolysis of the C−Br bond also takes place for single-molecule 5-BrU. Thus, 5-BrdU in solution has a short excited state lifetime of approximately 0.4 ps[13,14] and undergoes cleavage of the carbon−bromine bond upon UV irradiation with quantum yields of up to 5%.[15−17] However, also here the mechanism is unknown. Motivated by our interest in the UV sensitization of DNA with 5-BrU and its therapeutic potential, we have studied the photophysics and photochemistry of isolated 5-BrU with ab initio computations as a first step toward the elucidation of the photocleavage reaction mechanism in DNA.

SCHEME 1

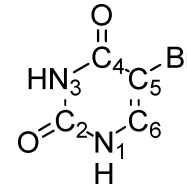

The CASPT2//CASSCF results (see Computational Methods) are summarized in Figure 1. Figure 1 is a sketch of the excited state energy surface along the two relevant nuclear coordinates, the C_5-Br distance and the out-of-plane bending angle of the bromine atom. The excited state surface is characterized by the absence of stable minima of the spectroscopically active (π,π^*) state, and after excitation the molecule is quickly deactivated toward an extended region of degeneracy or near-degeneracy between the first excited state and the ground state (S_1 and S_0, respectively). This is in agreement with the experimental short excited state lifetimes, since the region of degeneracy is energetically accessible from the Franck−Condon (FC) point,

* To whom correspondence should be addressed. E-mail: lluis.blancafort@udg.edu.
[†] University of Gdańsk.
[‡] Universitat de Girona.

10.1021/jp811330v CCC: $40.75
Published on Web 04/14/2009

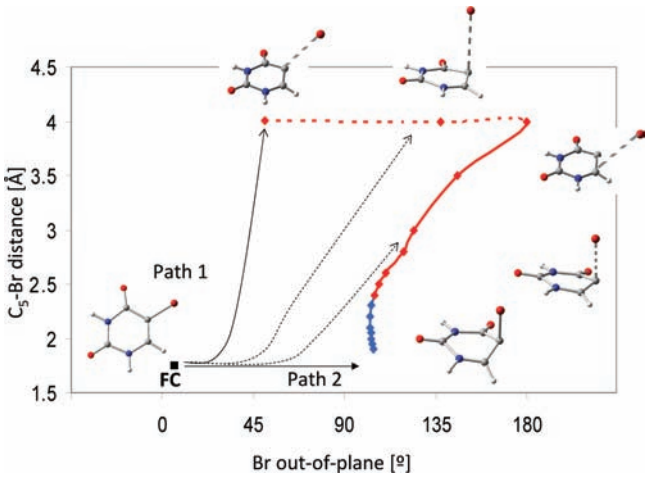

Figure 1. Projection of the S_1/S_0 degeneracy and near-degeneracy regions on the C_5-Br and Br out-of-plane coordinates. Full line: seam of intersection. Dotted line: near degeneracy. Color coding: red, photolysis; blue, reactant regeneration.

without substantial barriers. The degeneracy region lies along a combination of the two coordinates, and a large part (continuous line in Figure 1) corresponds to a seam of intersection between S_1 and S_0. The photoreactivity depends on which part of the region of degeneracy is reached by the excited molecule, where two different regions can be distinguished: one with short C_5-Br distances, where the decay leads to regeneration of the reactant (shown as a blue line in Figure 1), and one with long C_5-Br distances which can lead to photolysis (shown as a red line in Figure 1). The experimental photolysis quantum yield of up to 5% suggests that the access to the unreactive region of the seam is favored with respect to the photolysis region. Besides there is a third region of the seam, which is only partly shown in Figure 1, where the bromine atom shifts from the C_5 to the C_6 ring atom. As we will show in more detail below, no additional photoproducts are formed from this region.

Computational Methods

The calculations are carried out by using the CASPT2//CASSCF approach, where critical points and minimum energy paths are optimized at the CASSCF (complete active space self-consistent field) level, and the energies are recalculated at the CAPST2 (complete active space second-order perturbation) level to account for dynamic correlation. The CASSCF calculations have been carried out with Gaussian03,[18] and the CASPT2 calculations with Molcas7.0.[19] The 6-311G* basis set has been used throughout. The Supporting Information includes the CASSCF minimum energy paths from the FC structure and from several conical intersections.

Optimizations. The minimum energy paths from the FC structure and the conical intersection points have been calculated with the intrinsic reaction coordinate algorithm implemented in Gaussian,[20] using hypersphere geometry optimizations to determine the initial relaxation direction.[21] The paths are calculated with a step size of approximately 0.25 au, and the CASPT2 energies along the profile are calculated in steps of approximately 1 au. The relaxation path from the FC structure with a fixed C_5-Br distance has been calculated by freezing the corresponding internal coordinate. The calculated path is not a minimum energy path, but it is helpful to map the potential energy surface. To avoid active space orbital rotations along path 1, this path has been optimized by state-averaging the wave function over three states, optimizing the surface for the second root (see the Supporting Information). Points on the conical intersection seam (other than the minimum energy intersection) have been optimized constraining the C_5-Br or C_6-Br bond lengths (segments 1 and 2, respectively). For this purpose the calculations have been carried out on a version of Gaussian03 modified according the procedure described in ref 22, which has been generalized to nonsymmetric cases. The conical intersection optimization gradient in the unconstrained case is a sum of the projected excited state gradient, where the components along the branching space vectors are eliminated by projection, and a penalty term along the gradient difference vector.[23] In the modification implemented here, the projection of the excited state gradient is carried out with the constrained branching space vectors (transformed to redundant coordinates).

TABLE 1: CASPT2//CASSCF(16,12)/6-311G* Vertical Excitation Energies for 5-BrU

state	E_{exc} [eV][a]	f	leading config	characterization
S_1	5.1 (5.0)	3.8×10^{-1}	$\pi_1 \rightarrow \pi_1^*$	(π,π^*) (A′)
S_2	5.1 (5.0)	2.4×10^{-4}	$n_{O1} \rightarrow \pi_1^*$ $n_{O2} \rightarrow \pi_1^*$	(n_O,π^*) (A″)
S_3	5.7	4.4×10^{-3}	$\pi_1 \rightarrow \sigma^*$	(π,σ^*) (A″)
S_4	6.4 (6.3)	6.7×10^{-2}	$\pi_2 \rightarrow \pi_1^*$	(π,π^*) (A′)
S_5	6.5 (6.5)	2.7×10^{-7}	$n_{O1} \rightarrow \pi_2^*$ $n_{O2} \rightarrow \pi_2^*$	(n_O,π^*) (A″)
S_6	6.8	1.6×10^{-3}	$n_{Br} \rightarrow \sigma^*$	(n_{Br},σ^*) (A′)
S_7	7.0	2.5×10^{-6}	$n_{Br} \rightarrow \pi_1^*$	(n_{Br},π^*) (A″)

[a] For comparison, CASPT2//CASSCF(14,10)/6-311G* vertical excitation energies of thymine are shown in parentheses.

CASSCF Active Spaces. For the optimization of the minimum energy paths from the FC structure an active space of 12 electrons in 10 orbitals has been used (12,10), which includes 8 orbitals of the π system and two orbitals of the C−Br σ bond. For the optimizations on the conical intersection seam, it is necessary to reduce the active space to calculate the orbital rotation contribution to the gradients of the state-averaged states, by solution of the coupled-perturbed MCSCF equations.[24] Thus, the active space has been reduced to (8,7) by removing from the (12,10) space the π orbital with occupation closest to 2.0 and the two π orbitals approximately localized on the C_2-O_7 group. The reduced active space provides a balanced description of the excited and the ground state, as the energy degeneracy obtained at the CASSCF level of theory is kept at the CASPT2 level to within 0.1 eV. This validates the active space choice.

CASPT2 Calculations. To provide a consistent description of the energies, the CASPT2 energies have been calculated throughout with a (16,12) active space that includes, in addition to the (12,10) active space described above, the in-plane nonbonding orbital of the bromine atom and the π orbital approximately localized on the N_1 atom. The calculations are done by using a state-averaged six-root CASSCF wave reference function with equal weights for all states, a real level shift parameter of 0.2 au, and an IPEA parameter[25] of 0.25 au, which is the default in Molcas7.0. To determine the energies of the (n_O,π^*) excited states (excitation from the oxygen lone pairs), the calculations at the FC geometry and the first part of the decay path were repeated with a (16,12) active space where the π orbital with highest occupation and the in-plane nonbonding one of the bromine atom are replaced by the two oxygen lone pairs. In this case, five roots were included in the CASSCF calculation, averaging with equal weights. The vertical excitation energies presented in Table 1 have been obtained with one of these two (16,12) active spaces.

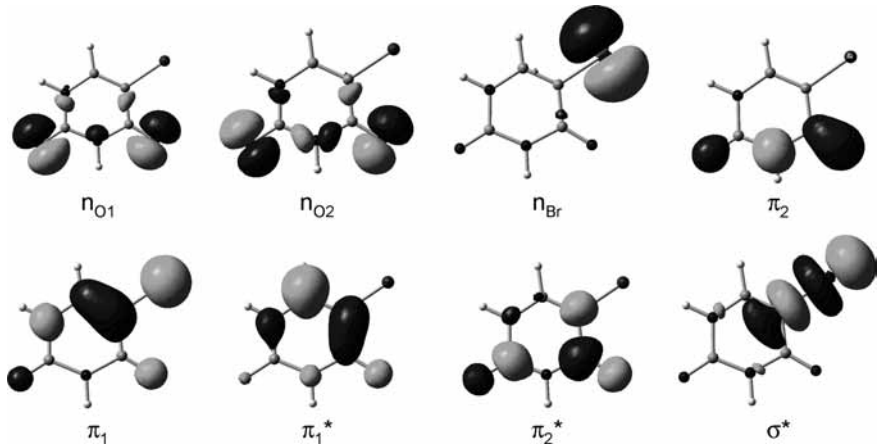

Figure 2. Orbitals involved in the vertical excitation.

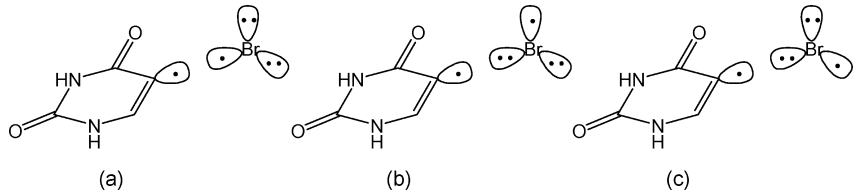

Figure 3. Resonance structures of near-degenerate states at the end of path 1. Correlation with vertical excited states: (a) ground state; (b) (π,σ^*); and (c) (n_{Br},σ^*).

Results and Discussion

Vertical Excitation Energies. The calculated vertical absorption spectrum for 5-BrU is presented in Table 1. The ground state minimum has C_s symmetry, and the symmetry of the excited states is indicated in the table. The orbitals involved in the excitation are displayed in Figure 2. The results for the (π,π^*) and (n_O,π^*) states are similar to the ones obtained for thymine and uracil at different levels of theory,[26−30] with the lowest (π,π^*) and (n_O,π^*) states being nearly degenerate at approximately 5.1 eV. This value is in reasonable agreement with the experimental absorption maximum of approximately 4.7 eV in the gas phase[31] and 4.5 eV in water.[32] In addition to these states, there is a low-lying (π,σ^*) state at 5.7 eV (excitation into the C−Br σ^* orbital) and two higher lying states at 6.8 and 7.0 eV where the excitation comes from the in-plane nonbonding bromine orbital.

The lowest (π,π)* state has significantly higher oscillator strengths than the other states. Therefore it is safe to assume that it is the one excited in the experiments conducted on 5-BrU in water and protic solvents, with excitation wavelengths that range from 266 to 254 nm (4.66 to 4.88 eV, respectively).[14,15,17] Because of the limitations of the active space, the Rydberg-like states, which appear at energies above 6 eV in uracil and have low oscillator strengths,[26] have not been calculated here. They should have similar energies and oscillator strengths in 5-BrU and play only a minor role in the low-energy photophysics.

Decay Paths from the FC Structure. Two decay paths from the FC structure have been calculated, starting on the lowest (π,π^*) state (S_1 at the FC geometry). The first path, shown as path 1 in Figure 1, is the CASSCF minimum energy path and corresponds to an adiabatic bond cleavage on S_1 where the process takes place on a single energy surface. At the planar FC structure, the value of the out-of-plane bending angle (defined as 180° minus the Br−C_5−C_4−N_3 dihedral angle) is 0°. The decay path is initially dominated by bond stretches in the ring and the out-of-plane bending of the bromine atom, but after an angle of approximately 20° is reached, the stretching of the carbon−bromine bond accompanies the bending. From the electronic structure point of view, the initial (π,π^*) excitation changes gradually to (π,σ^*) as the π^* and σ^* orbitals mix along the path. At the same time, the π orbital localizes on the bromine atom. At large C−Br distances, the photolysis products form a radical pair with three possible electronic configurations on the bromine atom (see Figure 3). The corresponding three states are virtually degenerate because of the small coupling between the two radical centers, and the three resonance structures shown in Figure 3 correlate with the ground state and the (π,σ^*) and the (n_{Br},σ^*) excited states (Figures 3, structures a, b, and c, respectively). Therefore, path 1 leads to a region of near-degeneracy between S_0, S_1, and S_2, where the states do not intersect but approach the degeneracy asymptotically, as the C−Br bond is stretched. This feature is shown on the CASPT2 energy profile along path 1 displayed in Figure 4. Moreover, although the CASSCF-optimized path corresponds to a barrierless decay, at the CASPT2 level there is a small barrier of approximately 0.2 eV. This is probably due to differences between the CASSCF and CASPT2 minimum energy paths, and not to a true minimum on the CASPT2 surface. In any case, the small barrier is lower than the excess energy provided by the vertical excitation, and the path should be energetically accessible.

The relatively small quantum yield of the photolysis[15] suggests that there is a competing, unreactive path for the decay. Such a path has been described for uracil and thymine.[33−38] It involves a conical intersection between the ground and excited states and is assumed to be responsible for the ultrafast decay of the excited states of these natural nucleobases. The path is characterized by an out-of-plane bending of the C_5 substituent. Thus, the C_5−C_6 double bond character is lost in the excited state, and the out-of-plane bending of the substituents is favored. At the same time, the ground state energy rises, and this induces the crossing of the two states. To investigate the possibility of

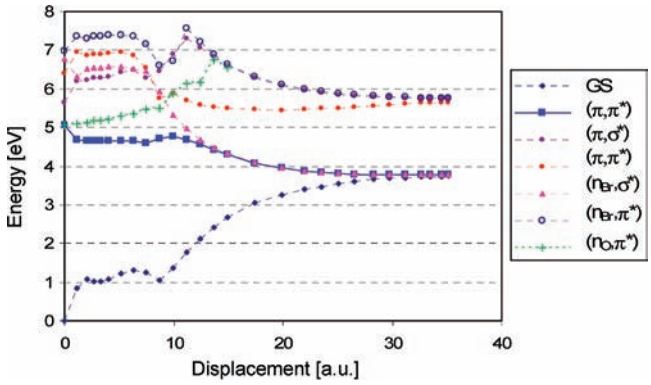

Figure 4. CASPT2//CASSCF(16,12)/6-311G* energy profile along path 1 (minimum energy path). The labels of the states refer to vertical excitations, but the character of the states changes along the path (see text).

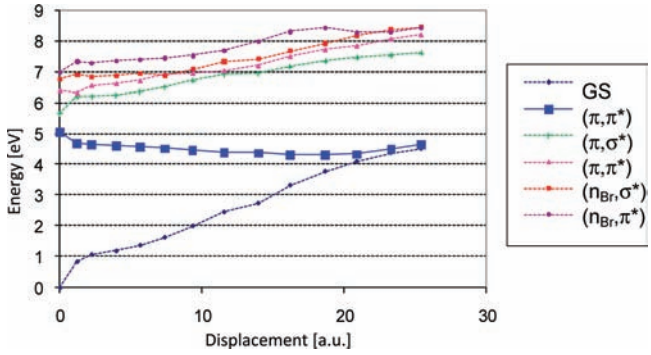

Figure 5. CASPT2//CASSCF(16,12)/6-311G* energy profile along path 2 (fixed C_5-Br distance). The labels of the states refer to vertical excitations.

an analogous decay mechanism for 5-BrU, the minimum energy path calculation from the FC structure has been repeated by freezing the C_5-Br distance to the initial value of 1.88 Å. This path, labeled path 2 in Figure 1, leads to a conical intersection with the ground state, and the CASPT2 energy profile of the excited state has only a small barrier (see Figure 5). Similar to what has been described for thymine and uracil,[33−38] the C_5 substituent is bent out of plane, and the C−Br bond is approximately perpendicular to the distorted uracil ring at the intersection.

The present approach used to study the relaxation process has some limitations. Thus, path 2 is not a conventional minimum energy path because an internal coordinate is fixed. However, paths 1 and 2 can be understood as limiting cases for the relaxation, and trajectories followed during the actual relaxation dynamics will be intermediate between paths 1 and 2. Besides, calculations for thymine and uracil have suggested that the (n,π*) state can be populated near the FC region during the decay of the close-lying (π,π*) state.[27,39,40] In the calculation of paths 1 and 2 for 5-BrU, the (n,π*) states have been neglected. However, the energy of the lowest (n,π*) state along path 1 was determined from single-point calculations (see Computational Methods and Figure 4). The energy of this state rises along path 1, and it can be expected to be even higher in protonated solvents,[27] where the experiments have been conducted. This supports the idea that the (n,π*) state is not directly involved in the photolysis.

Seam of Conical Intersection. The point of conical intersection encountered along path 2 is part of an extended seam along the C−Br stretching coordinate. The seam has two different

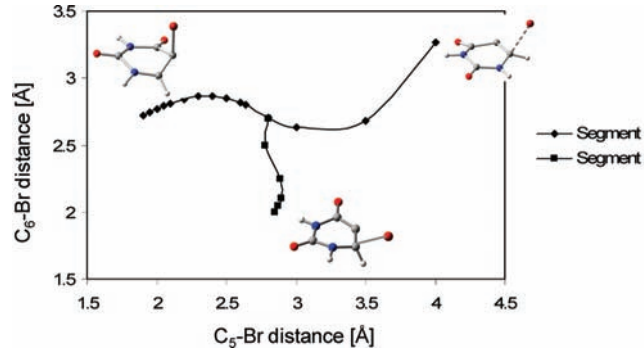

Figure 6. Projection of the S_1/S_0 seam of intersection on the C_5-Br and C_6-Br coordinates. Segment 1: constrained C_5-Br distance. Segment 2: constrained C_6-Br distance.

segments which have been characterized by optimizing several conical intersection structures fixing the C_5-Br and C_6-Br distances, respectively (see Computational Methods). Every point on Figures 1 and 6 corresponds to an optimized structure. The first segment is displayed as a solid line in Figure 1 as a function of the C_5-Br distance and the out-of-plane bending angle. Thus, at short C_5-Br distances ($r \leq 2.5$ Å), the out-of-plane bending angle of the conical intersection structures is approximately 100°, i.e., the C_5-Br bond is almost perpendicular to the ring. The deviation from the ideal value of 90° is due to small ring distortions. At longer C_5-Br distances, the angle increases because the bromine atom shifts toward the C_6 atom. The CASSCF minimum energy conical intersection lies on this segment, with a C_5-Br distance of 2.64 Å. A second segment of the seam lies along the C_6-Br stretch coordinate. The topology of this segment is plotted in Figure 6 as a function of the C_5-Br and C_6-Br distances, together with the first segment. The seam extends to structures where the bromine atom has migrated to the C_6 atom, leaving a carbene on C_5. The connection between the two segments is confirmed by comparing the structures obtained by constraining the C_5-Br distance to 2.8 Å and the C_6-Br distance to 2.5 Å.

The reactivity associated with the different regions of the seam has been studied by calculating the ground state decay paths from different points on the seam (see the Supporting Information). In the first segment of the seam, decay at the short C_5-Br distance region ($r_{C_5-Br} = 1.9$ Å) leads to the reactant, while at longer distances ($r_{C_5-Br} = 2.68$ Å) there are two decay paths, leading either to the reactant or to the dissociation products. Thus, the intersection changes from a sloped topology (one ground state decay path) to a peaked one (two paths) along the seam, similar to what has been described previously for fulvene.[22] Finally, decay at the second segment of the seam ($r_{C_6-Br} = 2.0$ Å) goes through an unstable carbene structure that is not a minimum on the potential surface. The decay is completed by a barrierless, reverse 1,2 shift of the bromine atom to C_5, leading to regeneration of the reactant. For comparison, CCSD(T)//B3LYP calculations (coupled cluster energies at geometries optimized with the hybrid Becke-3-Lee-Yang-Parr density functional) also predict that ethylidine, the carbene radical formed after the 1,2 hydrogen shift in ethylene, is an unstable species, with a barrier of less than 0.1 eV for the rearrangement back to ethylene.[41] The absence of a stable carbene after the bromine shift in 5-BrU is in agreement with this result.

The reactivity along the different segments can be rationalized with the help of the orbitals involved in the excitation. At short C_5-Br distances, the two orbitals in question are the π orbital

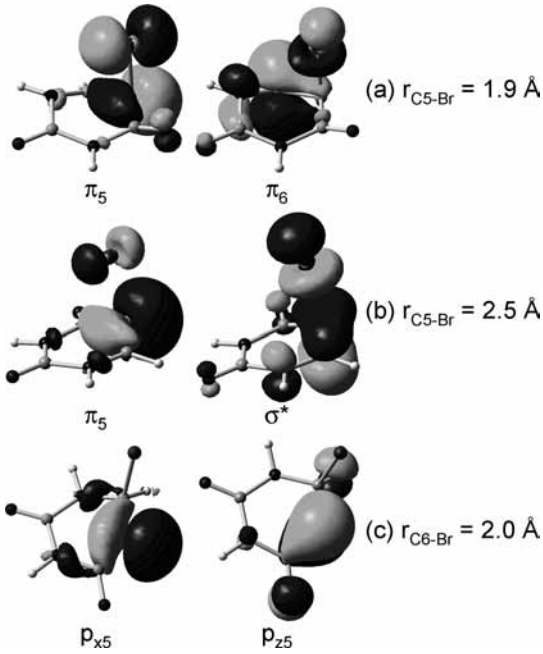

Figure 7. Orbitals involved in the excitation along the seam of intersection.

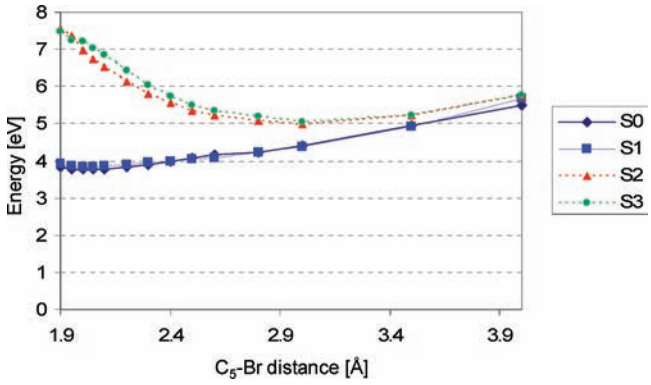

Figure 8. CASPT2//CASSCF(16,12)/6-311G* energy profiles along the seam of conical intersection (segment 1).

localized on C_5, which lies perpendicular to the plane of the ring because the substituent is bent out of the plane, and a π orbital largely localized on C_6 (see orbitals π_5 and π_6 in Figure 7a, respectively). The two intersecting states correspond to a diradical with configuration $(\pi_5)^1 (\pi_6)^1$ and a zwitterionic structure with configuration $(\pi_5)^2 (\pi_6)^0$. As the C_5-Br bond is stretched, the π_6 orbital mixes with the σ^* orbital of the stretched bond (see Figure 7b), and the diradical state turns to a dissociative (π,σ^*)-type state (configurations of the intersecting states: $(\pi_5)^2 (\sigma^*)^0$ and $(\pi_5)^1 (\sigma^*)^1$). Finally, along the second segment of the seam, the π_6 and C_5-Br σ orbitals mix (see Figure 7c), and the excitation localizes on the p_x and p_z orbitals of C_5, resulting in a formal carbene (configurations of the intersecting states: $(p_{x5})^2 (p_{z5})^0$ and $(p_{x5})^1 (p_{z5})^1$).

The energies of the four lowest states along the calculated S_1/S_0 seam segments are shown in Figures 8 and 9. The lowest energy part of the seam occurs for short C_5-Br distances ($r_{C-Br} \approx 2$ Å), where decay leads to the reactant (see Figure 8). However, the seam is energetically accessible for C_5-Br distances up to approximately 3.5 Å (energy lower than the vertical excitation of 5.1 eV), where dissociation can occur. In principle, also the second segment could be accessible from the point of view of its energy (see Figure 9), but this should have no consequence for the reactivity since no products are formed from that region.

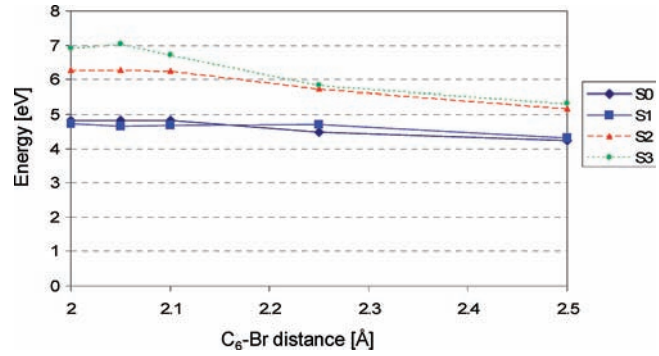

Figure 9. CASPT2//CASSCF(16,12)/6-311G* energy profiles along the seam of conical intersection (Segment 2).

Conclusions

The competition between the benign decay and the photolysis of 5-BrU can be rationalized on the basis of an extended region of degeneracy between S_1 and S_0. Two decay paths to access this region with small barriers have been mapped, one that leads to bromine elimination and one that leads back to the reactant (path 1 and path 2, respectively). Path 1 results in bromine elimination and leads to a region of near-degeneracy between the ground and excited states, and path 2 leads back to the reactant through a conical intersection between the two states. Although path 1 is the minimum energy path at the CASSCF level of theory, the CASPT2 energy profiles along both paths are similar. However, the relatively low quantum yield of the photolysis suggests that path 2 is favored. Moreover, the conical intersection for benign decay is part of a seam that lies along the C_5-Br stretching coordinate, and decay at the region of the seam with a stretched C_5-Br bond leads to photolysis. The bond cleavage can take place adiabatically, along trajectories similar to path 1, or along intermediate trajectories between paths 1 and 2 that lead to the reactive region of the seam of intersection.

From a general point of view, the key feature of the surface is the extended seam of intersection, which is composed of different segments associated with different reactivity. The changes in the reactivity are due to changes in the character of the excited state along the seam. This is a general feature of seams of conical intersection, and similar situations have been described for ethylene[42] and the excited state decay of the *keto* tautomer of *o*-hydroxybenzaldehyde.[43] In this respect, the space of the conical intersection has to be understood as an analogue of a Born−Oppenheimer surface, where different regions of the surface correspond to different chemical species. In the case of the conical intersection space, different regions of the seam lead to different photoproducts. To rationalize the ultrafast photophysical and photochemical processes it is therefore necessary to provide a full description of the seam of intersection along the different coordinates and characterize the decay paths associated with each region of the seam.

The analogy with the twisted conical intersection of ethylene[42,44−48] also regards the 1,2 shift coordinate. Similar to what is described here for 5-BrU, for ethylene it has been suggested that the twisted intersection forms part of a seam along the 1,2 hydrogen shift coordinate.[42] Recent ultrafast spectroscopy results also suggest that the 1,2 migration product of ethylene (ethylidine) is formed at the conical intersection seam as a short-

lived transient of approximately 1 ps lifetime before rearranging back to ethylene.[49] Our results on the decay of 5-BrU at the part of the seam associated with 1,2 migration suggest that a similar process is possible in 5-BrU, although the barrier to access that region should be established better to evaluate if the formation of the carbene transient actually takes place.

Turning to the photochemistry of 5-BrU, the results are in good agreement with the experimental excited state lifetimes and quantum yields of the reaction. The results also suggest that the bromine elimination takes place on an ultrafast time scale, during the decay to the ground state, and not as a result of hot vibrational states formed after internal conversion to the ground state. This is in contrast to what is generally assumed for ethylene[49,50] and is due to the lowering of the energy of the repulsive (π,σ*) state for the C−Br bond. The formation of bromine during the decay could be confirmed experimentally by detecting the 5-uracil radical in time-resolved experiments with sufficient resolution. The computations also allow us to suggest an alternative scenario to the bromine elimination in DNA containing 5-BrU, which is generally assumed to occur after a photoinduced electron transfer from an adjacent purine. Thus, in double-strand DNA the excitation is initially distributed along several stacked bases. Nuclear vibrations can induce a localization of the excitation on a single base. This can be inferred from the observation of a monomer-like decay component in excited DNA oligomers.[51] In DNA containing 5-BrU, localization of the excitation in the halogenated base can lead to bromine elimination without the preceding electron transfer. A crucial point to tell between the two mechanisms is the nature of the excited state accessed in the experiments in double-strand DNA containing 5-BrU, which is irradiated with a wavelength of approximately 300 nm or 4 eV.[4] This state could either be a charge transfer state to 5-BrU from an adjacent purine or a state delocalized over a few stacked bases. Calculations addressing this question will be the subject of future work.

Acknowledgment. This work was supported by the Spanish Dirección General de Investigación (MEC), grant CTQ2005-04563, the European COST Action P9 "Radiation Damage in Biomolecular Systems", Scientific and Technological International Cooperation Joint Project (MNiSW) Grant No. dec.127/02/E-335/S/2007 (J.R.), and the Polish State Committee for Scientific Research (KBN) Grant Nos. DS/8221-4-0140-9 and KBN/NN204 023135 (J.R.). D.A. acknowledges a MEC Ph.D. grant (FPU Grant No. AP2004-4774), A.M. acknowledges a fellowship from the Xarxa de I+D+i de Referència de Química Teòrica i Computacional de Catalunya, and M.K. acknowledges a grant from the High Performance Computing Europa Transnational Access Programne (no. 0659/2006). The research has been carried out using the facilities of the Catalan Centre for Supercomputation (CESCA).

Supporting Information Available: Complete ref 18 and CASSCF minimum energy paths, absolute energies, and Cartesian coordinates of relevant structures. This material is available free of charge via the Internet at http://pubs.acs.org.

References and Notes

(1) Friedberg, E. C.; Walker, G. C.; Sided, W.; Wood, R. D.; Schultz, R. A.; Ellenberger, T. *DNA repair mutagenesis*; ASM Press: Herndon, VA,2006.

(2) Chen, T. Q.; Cook, G. P.; Koppisch, A. T.; Greenberg, M. M. *J. Am. Chem. Soc.* **2000**, *122*, 3861–3866.

(3) Cook, G. P.; Chen, T. Q.; Koppisch, A. T.; Greenberg, M. M. *Chem. Biol.* **1999**, *6*, 451–459.

(4) Cook, G. P.; Greenberg, M. M. *J. Am. Chem. Soc.* **1996**, *118*, 10025–10030.

(5) Zeng, Y.; Wang, Y. S. *J. Am. Chem. Soc.* **2004**, *126*, 6552–6553.

(6) Zeng, Y.; Wang, Y. S. *Biochemistry* **2007**, *46*, 8189–8195.

(7) Cecchini, S.; Masson, C.; La Madeleine, C.; Huels, M. A.; Sanche, L.; Wagner, J. R.; Hunting, D. J. *Biochemistry* **2005**, *44*, 16957–16966.

(8) Szybalsky, W. *Cancer Chemother. Rep., Part 1* **1974**, *58*, 539–557.

(9) Blatter, E. E.; Ebright, Y. W.; Ebright, R. H. *Nature (London)* **1992**, *359*, 650–652.

(10) Dietz, T. M.; Koch, T. H. *Photochem. Photobiol.* **1989**, *49*, 121–129.

(11) Jensen, K. B.; Atkinson, B. L.; Willis, M. C.; Koch, T. H.; Gold, L. *Proc. Natl. Acad. Sci. U.S.A.* **1995**, *92*, 12220–12224.

(12) Willis, M. C.; Hicke, B. J.; Uhlenbeck, O. C.; Cech, T. R.; Koch, T. H. *Science* **1993**, *262*, 1255–1257.

(13) Lu, Q. B.; Baskin, J. S.; Zewail, A. H. *J. Phys. Chem. B* **2004**, *108*, 10509–10514.

(14) Wang, C. R.; Hu, A.; Lu, Q. B. *J. Chem. Phys.* **2006**, *124*, 241102.

(15) Campbell, J. M.; Schulte-Frohlinde, D.; von Sonntag, C. *Photochem. Photobiol.* **1974**, *20*, 465–467.

(16) Dietz, T. M.; von Trebra, R. J.; Swanson, B. J.; Koch, T. H. *J. Am. Chem. Soc.* **1987**, *109*, 1793–1797.

(17) Swanson, B. J.; Kutzer, J. C.; Koch, T. H. *J. Am. Chem. Soc.* **1981**, *103*, 1274–1276.

(18) Frisch, M. J. et al. *Gaussian03*, Revision B.02 ed.; Gaussian, Inc.: Pittsburgh, PA, 2003.

(19) Karlström, G.; Lindh, R.; Malmqvist, P.-Å.; Roos, B. O.; Ryde, U.; Veryazov, V.; Widmark, P.-O.; Cossi, M.; Schimmelpfennig, B.; Neogrady, P.; Seijo, L. *Comput. Mater. Sci.* **2003**, *28*, 222–239.

(20) González, C.; Schlegel, H. B. *J. Phys. Chem.* **1990**, *94*, 5523–5527.

(21) Celani, P.; Robb, M. A.; Garavelli, M.; Bernardi, F.; Olivucci, M. *Chem. Phys. Lett.* **1995**, *243*, 1–8.

(22) Bearpark, M. J.; Blancafort, L.; Paterson, M. J. *Mol. Phys.* **2006**, *104*, 1033–1038.

(23) Bearpark, M. J.; Robb, M. A.; Schlegel, H. B. *Chem. Phys. Lett.* **1994**, *223*, 269–274.

(24) Yamamoto, N.; Vreven, T.; Robb, M. A.; Frisch, M. J.; Schlegel, H. B. *Chem. Phys. Lett.* **1996**, *250*, 373–378.

(25) Ghigo, G.; Roos, B. O.; Malmqvist, P. A. *Chem. Phys. Lett.* **2004**, *396*, 142–149.

(26) Fleig, T.; Knecht, S.; Hättig, C. *J. Phys. Chem. A* **2007**, *111*, 5482–5491.

(27) Gustavsson, T.; Banyasz, A.; Lazzarotto, E.; Markovitsi, D.; Scalmani, G.; Frisch, M. J.; Barone, V.; Improta, R. *J. Am. Chem. Soc.* **2006**, *128*, 607–619.

(28) Schreiber, M.; Silva, M. R.; Sauer, S. P. A.; Thiel, W. *J. Chem. Phys.* **2008**, 128.

(29) Shukla, M. K.; Leszczynski, J. *J. Comput. Chem.* **2004**, *25*, 768–778.

(30) Silva, M. R.; Schreiber, M.; Sauer, S. P. A.; Thiel, W. *J. Chem. Phys.* **2008**, *129*, 104013.

(31) Abouaf, R.; Pommier, J.; Dunet, H. *Chem. Phys. Lett.* **2003**, *381*, 486–494.

(32) Campbell, J. M.; von Sonntag, C.; Schulte-Frohlinde, D. *Z. Naturforsch.* **1974**, *29*, 750–757.

(33) Hudock, H. R.; Levine, B. G.; Thompson, A. L.; Satzger, H.; Townsend, D.; Gador, N.; Ullrich, S.; Stolow, A.; Martinez, T. J. *J. Phys. Chem. A* **2007**, *111*, 8500–8508.

(34) Matsika, S. *J. Phys. Chem. A* **2004**, *108*, 7584–7590.

(35) Merchán, M.; González-Luque, R.; Climent, T.; Serrano-Andrés, L.; Rodríguez, E.; Reguero, M.; Peláez, D. *J. Phys. Chem. B* **2006**, *110*, 26471–26476.

(36) Perun, S.; Sobolewski, A. L.; Domcke, W. *J. Phys. Chem. A* **2006**, *110*, 13238–13244.

(37) Zechmann, G.; Barbatti, M. *J. Phys. Chem. A* **2008**, *112*, 8273–8279.

(38) Zgierski, M. Z.; Patchkovskii, S.; Fujiwara, T.; Lim, E. C. *J. Phys. Chem. A* **2005**, *109*, 9384–9387.

(39) Mercier, Y.; Santoro, F.; Reguero, M.; Improta, R. *J. Phys. Chem. B* **2008**, *112*, 10769–10772.

(40) Serrano-Pérez, J. J.; González-Luque, R.; Merchán, M.; Serrano-Andrés, L. *J. Phys. Chem. B* **2007**, *111*, 11880–11883.

(41) Chang, A. H. H.; Mebel, A. M.; Yang, X. M.; Lin, S. H.; Lee, Y. T. *Chem. Phys. Lett.* **1998**, *287*, 301–306.

(42) Barbatti, M.; Paier, J.; Lischka, H. *J. Chem. Phys.* **2004**, *121*, 11614–11624.

(43) Migani, A.; Blancafort, L.; Robb, M. A.; Debellis, A. D. *J. Am. Chem. Soc.* **2008**, *130*, 6932–6933.

(44) Buenker, R. J.; Bonačić-Koutecký, V.; Pogliani, L. *J. Chem. Phys.* **1980**, *73*, 1836–1849.

(45) Ohmine, I. *J. Chem. Phys.* **1985**, *83*, 2348–2362.

(46) Bonačíć-Koutecký, V.; Koutecký, J.; Michl, J. *Angew. Chem., Int. Ed. Engl.* **1987**, *26*, 170–189.
(47) Freund, L.; Klessinger, M. *Int. J. Quantum Chem.* **1998**, *70*, 1023–1028.
(48) Ben-Nun, M.; Martinez, T. *J. Chem. Phys.* **2000**, *259*, 237–248.
(49) Kosma, K.; Trushin, S. A.; Fuss, W.; Schmid, W. E. *J. Phys. Chem. A* **2008**, *112*, 7514–7529.
(50) Chang, A. H. H.; Hwang, D. W.; Yang, X. M.; Mebel, A. M.; Lin, S. H.; Lee, Y. T. *J. Chem. Phys.* **1999**, *110*, 10810–10820.
(51) Crespo-Hernández, C. E.; Cohen, B.; Kohler, B. *Nature (London)* **2005**, *436*, 1141–1144.

JP811330V